

Multi-Tones' Phase Coding (MTPC) of Interaural Time Difference by Spiking Neural Networks

Zihan Pan, Malu Zhang, Jibin Wu, and Haizhou Li, *Fellow, IEEE*

Abstract—Inspired by the mammal's auditory localization pathway, in this paper we propose a pure spiking neural network (SNN) based computational model for precised sound localization in the noisy real-world environment, and implement this algorithm in a real-time robotic system with microphone array. The key of this model relies on the MTPC scheme, which encodes the interaural time difference (ITD) cues into spike patterns. This scheme naturally follows the functional structures of human auditory localization system, rather than artificially computing of time difference of arrival. Besides, it highlights the advantages of SNN, such as event-driven and power efficiency. The MTPC is pipeliend with two different SNN architectures, the convolutional SNN and recurrent SNN, by which it shows the applicability to various SNNs. This proposal is evaluated by the microphone collected location-dependent acoustic data, in a real-world environment with noise, obstruction, reflection or other affects. The experiment results show a mean error azimuth of $1^\circ \sim 3^\circ$, which surpasses the accuracy of the other biologically plausible neuromorphic approach for sound source localization.

Index Terms—neural phase coding, spiking neural network, sound localization

I. INTRODUCTION

The ability to detect the source of sounds is one of the most crucial skills of surviving in dynamic environments for humans or other mammals [1]. It helps to locate the prey, escape from the predators, find mates, or perform other activities. The location-dependent sounds or acoustic stimulus naturally contain redundant localization information and are sensed by the ears, encoded into neuronal spiking form of cues, and decoded into azimuths along the auditory pathways, including the auditory peripheral system and mid-brain cortex [2].

Date back to one century ago, people started the research of auditory perception of space [3] [4], from then on we know that the mammalian auditory localization systems benefit from two major cues: the interaural time difference (ITD) and the interaural intensity difference (IID), which are known as “duplex theory of sound localization”. Assuming a sound source locating at the left side, the sound emitted by it will arrive at the left ear before the right ear, as well as stimulates stronger neuronal responses in the left ear. Such a propagation time delay difference or sound pressure level decaying difference can provide the information for locating the azimuth of the sound source at some spatial resolution. The ITD and IID cues are extracted in the medial superior olive (MSO) [5] and lateral superior olive (LSO) [6], respectively. They have different working frequencies, for example, low frequencies

(in humans 20Hz to 2kHz) for MSO and high frequencies (in humans >2 kHz) for LSO [7]. From the information flow point of view, the location-dependent information from the sounds, or aforementioned time or intensity differences, are encoded into spiking pulses in the MSO and LSO. After that, they are projected to the inferior colliculus (IC) in the mid-brain, where the IC integrates both cues for estimating the sound source direction [8]. The most successful model for ITD encoding in MSO and cortex decoding might be the “place theory” by an American psychologist named Lloyd Jeffress [9], which is also referred to as Jeffress model hereafter.

In this theory, there are a series of nerve fibers with different synaptic delays used as “delay lines” and a coincidence detector used to detect the synchronization between binaural inputs. A distribution of spiking rates indicating the azimuth, so-called “place map” is generated from the synchronizing detection. By the processing, the binaural acoustic inputs are encoded into a spike pattern with ITD cues embedded. Such theory is biologically evaluated by the evidences of the “place map” or “ITD map” later found in barn owl [10] [11]. For the LSO encoding intensity difference, various models are also proposed. The LSO has a much smaller neuronal scale compared with the MSO (10,000-11,000 vs 2,500-4,000 neurons, [12]). Furthermore, the ITD cue encoded by MSO achieves a localization resolution as high as $1^\circ \sim 2^\circ$ [13], which is sufficient for real-world application. Therefore, for our computational model in this paper, we will extend the original Jeffress MSO model and propose a novel ITD-based encoding/decoding scheme for the real-world robust sound localization, together with a spiking neural network.

Above all, those aforementioned theories or models, from the encoding pathways to the decoding mid-brain cortex, are biologically plausible, which are based on the temporal-related spiking neuronal systems. On the other hand, from the engineering application point of view, the spiking neuronal models can also offer additional engineering advantages, such as ultra-low power consumption and high-speed processing. The spiking neural networks (SNN) are believed to be the third generation of the neural network, compared with the traditional artificial neural network. Plenty of pieces of evidence and applications have proved the effectiveness and efficiency in different cognitive applications, such as computer vision, automatic speech recognition, etc. As such, both the biological findings on the neuronal pathway for sound localization and the SNN advantages on application motivate us to combine them together and propose a novel spiking computational model for the real-world application.

Although the neuronal circuit for encoding the binaural

Zihan Pan and Malu Zhang contributed equally in this work, and should be regarded as co-first authors.

Jibin Wu is the corresponding author.

localization cues and neuronal processing are characterized physiologically [14] [15], which might be one typical case which the humans understand well about the behavioral function of a circuit in the central nervous [8], we are still lacking good computational models that are capable of robustly solving real-world applications. Furthermore, these remarkable scientific findings can hardly tell us the realization in engineering applications, but they provide inspiration and in-depth understanding.

Fortunately, some researchers have stepped forward to propose various SNN models for sound localization applications and positive results are provided. Experimentally derived head-related transfer function (HRTF) acoustical data from adult domestic cats were employed to train and validate the localization ability of the architecture [7]. This work is built on the earlier work of [16], [17]. They propose a model that encodes the IID cues into the spike rates of LSO neurons and learns the spike patterns with ReSuMe rule [18]. It achieves $\sim 10\%$ error rates with an error tolerance of $\pm 10^\circ$. However, the validation sounds are single-frequency tones of 5kHz, 15kHz, and 25kHz without noise. Similar works by simulated pure tones are also reported [19] [20] [21]. On the other hand, studies on ITD encoding by MSO are also presented. For example, Voutsas et al. [22] propose a binaural sound source lateralization neural network (BiSoLaNN) that utilizes a single delay line to encode the ITD cues similar to the Jeffress model. This model achieves the best localization accuracy of 72.5% in the range of $\pm 45^\circ$ with an error tolerance of $\pm 15^\circ$. However, the evaluation sounds are low-frequency pure tones between 440Hz and 1240Hz.

According to the “duplex theory of sound localization”, some of the researchers try to combine both cues together. One of the representative studies carried out by Liu et al. [23], proposes a more biologically plausible SNN-based computational model, which encodes both ITD and IID cues to imitate the functions of MSO and LSO neurons, respectively. To reflect the biological organization, the MSO and LSO have separated working frequency bands ($< 1\text{kHz}$ and $1\text{--}4\text{kHz}$). The duplex cues are combined in the IC model, in which it is assumed that the strengths of inputs from MSO and LSO are proportional to the posterior probabilities of the estimated azimuths, that are mathematically calculated by Bayesian theorem. The evaluation dataset is the microphone recorded stereo sounds of five spoken English words. It achieved 90% localization accuracy for sounds between $\pm 45^\circ$ with a spatial resolution of 10° , but the performance dropped dramatically when sounds moving to the sides, which means this model can hardly locate the sounds near extreme positions ($\pm 90^\circ$). Interestingly, this work is extended to combine with an automatic speech recognition system on a robot system [24], to help further improve the speech recognition accuracy.

Except for directly encoding the duplex cues, some other works offer different views of bio-inspired sound localization mechanisms. Goodman et al. [25] propose that our neuronal system locates the sound source by mapping the binaural location-specific sounds to two synchronous spiking patterns, which are derived from spatio-temporal filtering and spiking nonlinearity, and thus stimulating the activation of location-

specific assemblies of postsynaptic IC neurons. In the more recent works, they extend this idea to a learnable, self-adaptive, and noise-robust model [26] [27] using Hebbian learning. The experiment results show a mean absolute error of $10^\circ \sim 30^\circ$.

Those aforementioned studies successfully offer novelties in different aspects, such as binaural cues encoding/decoding, or classification back-ends. By summarizing all those works above, we find several common challenges among them, which build a limitation to a more effective and robust neuromorphic approach for real-world sound localization applications:

- 1) Most of the models or architectures are evaluated by the simulated localization datasets. Such datasets are artificially generated by convolving the single-channel audio recordings or pure tones with binaural or multi-channel head-related transfer functions (HRTF) [16], [17], [19]–[21]. When applied in real-world recorded sounds, the localization accuracy drops a lot [22], [26], [27].
- 2) In the application, reliable localization accuracy is only achieved in a small detecting region ($\pm 60^\circ$) [20], [23], or the spatial resolution is not sufficiently high ($20^\circ \sim 30^\circ$) [7], [22].
- 3) Although some works achieve relative good performances, they do not propose purely biologically plausible SNN models with spiking-involved either encoding front-end or decoding back-end [23] [20].
- 4) Most of the models cannot be extended to multiple channels, which is a limitation of the binaural model. Bio-inspired engineering systems always learn from nature and are expected to surpass it.

As such, our main contribution in this paper is that we propose a computational model with MTPC front-end and SNN-based learning architecture, for the precise and robust sound localization application in the real-world environment. We use the recorded sounds from a microphone array of four mics, and encode the time differences from each pair of microphones into the spike rates of an assembly of MSO neurons. Then the encoded spikes are fed into different deep architectures of SNNs. By using this model, our system could locate the sound source from 360° with a spatial resolution of 5° . Besides, the MTPC is independent of the temporal synaptic learning rules, as well as of the SNN architectures. So it is friendly to pipeline with most of the existing SNN classifiers.

The rest of this paper is organized as follows: in Section II we propose the MTPC scheme to encode ITD cues into spikes. In Section III the recurrent and convolutional architectures of SNN are introduced to learn the spike patterns and estimate the sound source azimuth. Section IV introduces our integrated SSL computational model, the collected dataset by microphone array, as well as the results in various experimental conditions. Discussion and conclusion are in Section V and VI.

II. NEURAL PHASE ENCODING OF ACOUSTIC STEREO INFORMATION

A. Neural Mechanisms of Coding Interaural Time Differences: the classical Jeffress Model

The scene, in which creatures localize the sounds from some particular source by the interaural time difference, can be

mathematically formulated as a 2-D sound direction estimation problem, demonstrated in Figure 1. The sound source emits sound, which travels in the form of mechanical vibration through the air and arrives at two ears separately. The environment includes the air, acoustic noise, obstacles, or acoustic reflectors, that jointly compose the acoustic transmission channel. As such, the received acoustic stimulus by the two ears will suffer different time delay and energy attenuation, which reflects in the changing of phases and amplitudes of the signals.

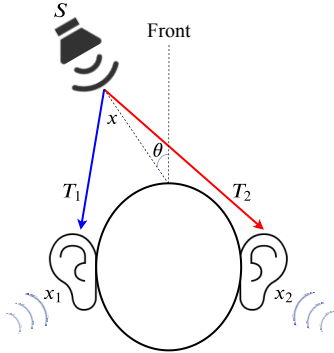


Figure 1. Binaural sound source localization problem: a sound source S locates in front of a person's head, θ degree to the left, and emits a sound signal x . x travels through two different pathways (indicated by blue and red arrows) to the left and right ears, becoming x_1 and x_2 , due to suffering different propagation delay, amplitude attenuation, phase distortion, etc. The corresponding propagation times are T_1 and T_2 , respectively. Our goal is to estimate the sound source azimuth θ from the received distorted sounds x_1 and x_2 , by a spiking neuromorphic approach without any prior knowledge of the transmission channels or other information.

The sounds from left and right pathways, filtered by the transmission channel, contain the ITD cues implicitly. To estimate the sound source direction, the mammals have evolved an auditory structure known as “delay line” in the MSO organ, proposed by Lloyd Jeffress, to encode the mechanical vibrations into electrical pulses. The Jeffress model [9] has become the dominant ITD encoding model since 1948, as demonstrated in Figure 2. The binaural sound waves travel through the pathways of the ipsilateral ear and contralateral ear. Since the sound source occurs at the ipsilateral side, the mechanical vibrations will arrive at the contralateral ear later than the ipsilateral ear. The time difference between the two ears, usually referred to as time difference of arrival (TDOA), is detected by the “delay line” structure. The sound at the ipsilateral side ear, referred to as acoustic stimulus in the auditory pathway, passes through a series of neural fiber with different synaptic delays and goes into the coincidence detection neurons in parallel. Once the ipsilateral acoustic stimulus plus some particular delay and the contralateral one arrive at the detection neuron simultaneously, the detection neuron with the particular synaptic delay will fire significantly more spikes. As such, the “delay line” model successfully represents the time difference as a firing rate distribution along the detection neurons.

From the computational neuroscience point of view, in principle, the place theory of encoding ITD is to project the time difference onto the spatial domain, which is detected

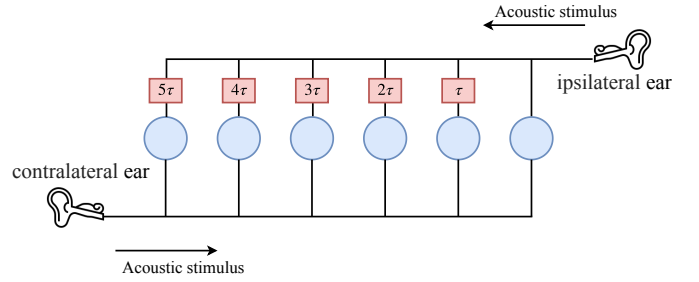


Figure 2. Jeffress model of ITD encoding. The sound from a specific location source arrives at two ears separately with different propagation times. The sounds go through each delay line (red boxes), and the blue neuron works as a coincidence detector. For example, let us consider a case where a sound source locates at the left side of 60° , the sound wave is supposed to arrive at the left ear assuming 3τ earlier than the right ear, where τ is the smallest processing time unit. As such, the acoustic signal arrived at the right ear will travel through the detector neuron with a synaptic delay of 3τ and meet the one at the left ear simultaneously, which stimulates that neuron to emit significantly more spikes. On the contrary, the detection neurons with other delays will fire little. Such a distribution of firing rates indicates the TDOA between the left and right ears.

and encoded by a population of neurons. However, this model only offers a prototype of ITD encoding from anatomy. Many models are raised for the application of sound localization, according to the place theory. Among them, however, many problems exist as mentioned in Section I. So we aim to propose a novel place theory-based neuromorphic computational model that is competitive in the real-world application.

B. Multi-Tones' Phase Coding (MTPC) of ITD localization cues

Figure 3 illustrates the MTPC for ITD. This neural spike encoder consists of three main components: the frequency analyzer (b), the phase encoder (c), and the coincidence detector (d).

1) *Frequency analyzer*: Evidence has been provided to prove that our auditory system is primarily a frequency analyzer, in which cells of the basilar membrane are found to respond to different vibration frequencies. Inspired by these acoustic and anatomical findings, our proposed encoder designing begins with a frequency analyzer that decomposes the acoustic input into pure tones with single frequencies, as demonstrated in Figure 4. In the mathematical implementation, the Fast Fourier Transform (FFT) is used for frequency analysis. Supposing the input sound signal $\mathbf{x} = [x_1, x_2, \dots, x_T]$ with sampling frequency f_s , either for left or right ear, is decomposed by N -point FFT into an N -length complex Fourier series denoted by $\mathcal{F}(\mathbf{x})$:

$$\begin{aligned} \mathcal{F}(\mathbf{x}) &= [a_1 + jb_1, a_2 + jb_2, \dots, a_N + jb_N] \\ &= [A_1 e^{j\phi_1}, A_2 e^{j\phi_2}, \dots, A_n e^{j\phi_n}, \\ &\quad A_{n+1} e^{j\phi_{n+1}}, \dots, A_{2n} e^{j\phi_{2n}}] \end{aligned} \quad (1)$$

Each complex value (i.e. $a_1 + jb_1$) from the Fourier series $\mathcal{F}(\mathbf{x})$ has the physical meaning of the amplitude and initial phase of the corresponding pure tone with a certain analysis frequency. So it is more clear to rewrite them into the form of polar coordinate, such as $A_1 e^{j\phi_1}$, in the second row of Eq.1.

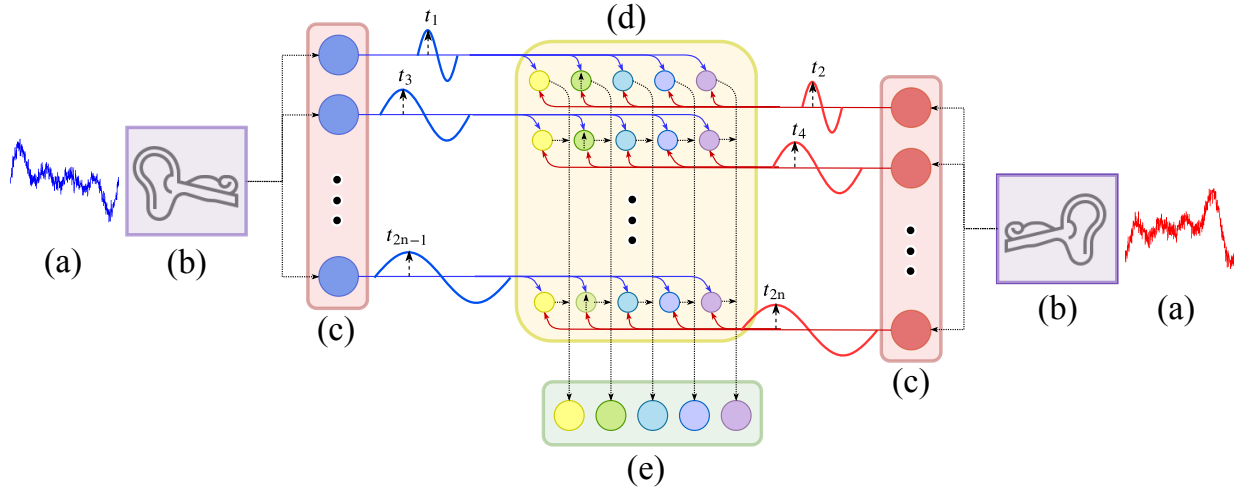


Figure 3. Diagram of the three-layer architecture of MTPC for sound localization. The binaural sounds (a) are decomposed into pure tones by frequency analysis in the basilar membrane of the cochlea (b). The spike timings are phase-locked to the first peak of each tone, as indicated by the dash arrows in (c). The phase-locked spike timings are put into the assembling of the coincidence detector neurons (d). For each frequency, only the neuron with a particular synaptic delay that detects the coincidence between the two input spikes will emit a spike to the next layer. In the output neuron layer (e), all the spikes from the coincidence detector neurons belonging to the assembly with the same delay are summed up. The spike rates (number of spikes) constitute the final encoded spike pattern that contains the ITD cues from binaural inputs.

Since the FFT results in the analysis bandwidth from 0 to the Nyquist frequency, which is twice higher than the signal's bandwidth, we only need the first half of the $\mathcal{F}(x)$ vector and ignore the symmetric half. As such, the frequencies of the decomposed pure tones are: $[\frac{1}{N}, \frac{2}{N}, \dots, \frac{n}{N}] * fs$, and $n = N/2$.

For the i^{th} ($i = 1, 2, \dots, n$) pure tone, we are able to acquire the analytical expression of the time-domain waveform $y_i(t)$ according to the analysis above:

$$\begin{aligned} y_i(t) &= A_i \sin(2\pi f_i t + \phi_i) \\ f_i &= \frac{i}{N} f_s \\ A_i &= \sqrt{a_i^2 + b_i^2} \\ \phi_i &= \tan^{-1}(b_i/a_i) \end{aligned} \quad (2)$$

2) *Neural phase encoder*: The pure tones, obtained from the decomposing of input sounds by the basilar membrane and frequency-sensitive cells, are encoded into spikes by the auditory nerves in the organ of Corti, which are the electrical pulses transmitted and processed in the spiking neural network. As illustrated in Figure 4, also in Figure 3(c), the spike timings are encoded as the first peak of each analytical pure tones. This is one sort of neural phase coding, which makes the spike timings phase-locked to a fixed phase timing. In this case, the sinusoidal oscillation of acoustic pure tones is phase-encoded by being locked to the peaks. Assuming a pair of pure tones from the left and right ears, $y_1^L(t)$ and $y_1^R(t)$, which has frequency $f_1 = \frac{1}{N} f_s$ and initial phases $\phi_1^L = \tan^{-1}(b_1^L/a_1^L)$, $\phi_1^R = \tan^{-1}(b_1^R/a_1^R)$, the corresponding phase encoding neurons will fire spikes at t_1 and t_2 :

$$\begin{aligned} t_1 &= (\pi + \tan^{-1}(b_1^L/a_1^L))/2\pi f_1 \\ t_2 &= (\pi + \tan^{-1}(b_1^R/a_1^R))/2\pi f_1 \end{aligned} \quad (3)$$

This first-peak phase coding has several advantages. First, we do not need to encode every peak, which is commonly done

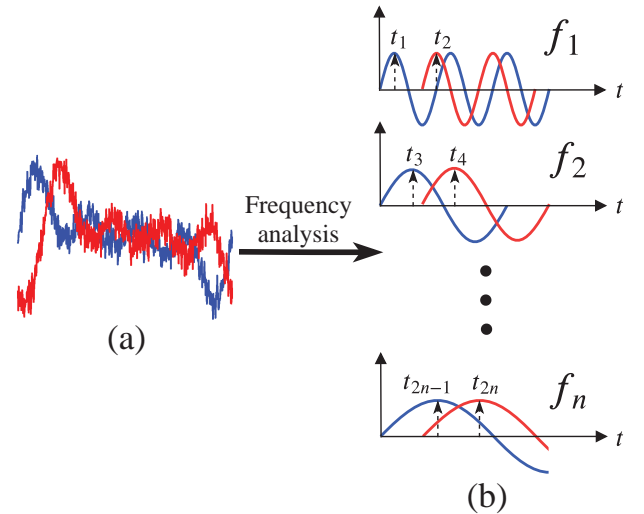


Figure 4. Neural phase encoder. The distorted binaural sounds (a) are analyzed in the frequency domain and decomposed into pure tones with frequencies from f_1 to f_n , as shown in (b). Blue and red curves represent the sounds received by the left and right ear, respectively. As described in Figure 1, the sound source locates at the left side, so the red curve has some delay to the left curve. Taking the f_1 tones as an example, the encoding neurons detect the energy peaks of the oscillation and emit spikes at the first peaks, which are time t_1 and t_2 . Each pure tone has one corresponding phase encoding neuron. The spike timings t_1 and t_2 embed the ITD cues to be further extracted.

in phase-locking encoding. It is because the first peaks contain sufficient temporal cues for ITD encoding. Then the first-spike encoding has more energy efficiency than other normal phase codings, the coding efficiency has always been one important aspect of neural encoding front-ends. Lastly, the pure tones are significant, because each pair of pure tones with the same frequency are coherent. From the signal processing point of view, coherent waves are easier for temporal delay detection, signal correlation tasks, compared to complex signals with

mixed frequencies. Besides, the phase-locking encoding is also well supported by biological observations.

3) *Coincidence detector*: The last step of the MTPC scheme is the coincidence detection for every pair of phase-coded spike patterns. The detection process also works purely by the transmission of spikes. The schematic diagrams are shown in 3(d), and a detailed illustration Figure 5. Coincidence detection aims to extract the ITD information embedded in the phase-coded spikes and represent it in the form of temporal spikes.

In this process, each pair of phase-coded spikes (refer to Figure 3(c)), distinguished by different frequencies, forward into the coincidence detection network (Figure 3(d)), and the network outputs spike patterns from Figure 3(e).

For instance in Figure 5(a), one pair of binaural location-dependent sounds are decomposed into 4 pairs of pure tones, and they are further phase-encoded into 4 pairs of spike trains: $[t_1, t_2], \dots, [t_7, t_8]$. Assuming that the spike timings with even subscripts are first arriving as in the reference side, the four pairs of spike trains are forwarded into the coincidence detection network. In this network, each row of neurons represents one unique frequency, and each column of neurons with a unified color represents the ITD detection by compensating one unique TDOA. In this noiseless example, the delay of each frequency is all τ_2 , such that every row detects the delay of τ_2 and drives the green color neuron firing a spike (black arrows in Figure 5).

The symmetric architecture of the coincidence detection is found in the auditory pathway of mammals, since the compensated delay is naturally a positive real value. However, in the engineering system, negative delay values are implementable. So we apply one coincidence detection network in the engineering realization, instead of the symmetric architecture with two networks, to simplify the computational model and engineering system.

The output spikes of the coincidence detection network organize a 2-D distribution of various frequencies on the pre-defined TDOA range ($\tau_1 \sim \tau_5$). This is a binary matrix in which 1 indicates one spike is fired during the analysis window. According to the topology of the coincidence detection network (Figure 3(d)), the column and row index of each spike on the map figures out the estimation of a particular delay on a certain frequency.

4) *Output layer of MTPC*: In the final step, the pure tones are grouped into sub-bands in subject to the centre frequencies and bandwidths of human cochlear filter bank, as demonstrated in Figure 6. For each sub-band, we sum up the number of spikes along the columns to form a 1-D distribution of estimated delay times. All the 1-D sub-band distribution are stacked over to generate a 2-D pattern (Figure 6(b)): one dimension of frequency channel and one dimension of estimated TDOA.

Figure 7 illustrates the outputs of the MTPC scheme, by inputting binaural sounds of real-world collected from different azimuths. 40 cochlear channels are utilized in the output layer. The distribution of TDOA on various azimuths is roughly observable.

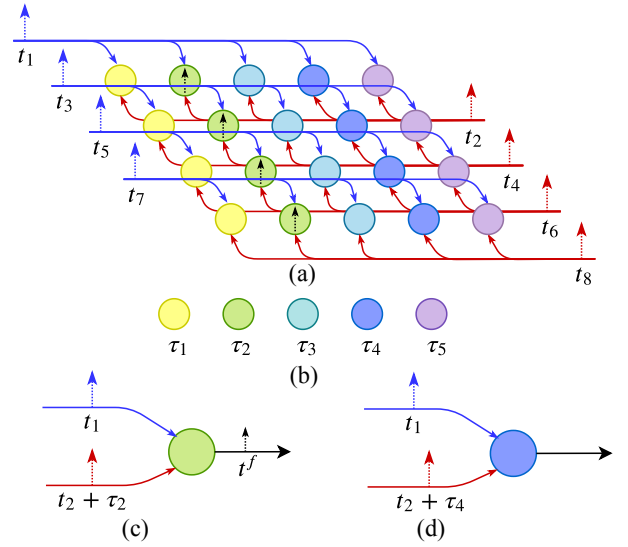


Figure 5. Coincidence detection network. The coincidence detection network (a) is composed of different sorts of detection neurons varying in synaptic delays. In this case, five neurons are illustrated in (b). Each sort of neurons have two input afferents to receive the inputs from two ears, shown as the blue and red lines, and one of the afferents has one unique and fixed synaptic delay time. The blue line afferent is designed as a reference line without delay, while the red line has a synaptic delay, varying from τ_1 to τ_5 . Each detection neuron will fire a spike if the two spikes arrive at the soma of the neuron simultaneously. For instance, in (c) the spike t_1 from the reference ear arrives at time of t_1 without delay, while the spike t_2 from the other side arrives at time of $t_2 + \tau_2$ after a delay of τ_2 . Coincidentally they meet at the soma simultaneously with $t_1 = t_2 + \tau_2$, such that this neuron (c) detects the coincidence and fires a spike. On the other hand, for instance in (d), the neuron will keep silent if the two spikes miss each other with $t_1 \neq t_2 + \tau_4$.

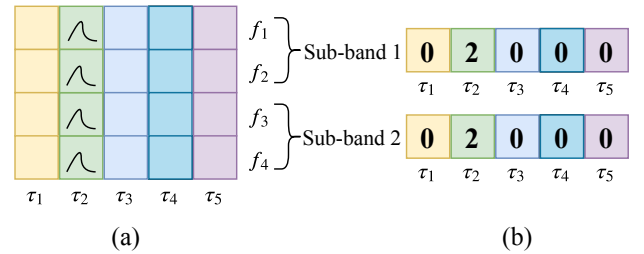


Figure 6. The output layer of MTPC. The 2-D output pattern (a) from Figure 3(d) will be selectively row-wisely grouped by the frequency channels according to the human cochlear filter bank. The sub-band spike temporal information is represented by the number of spikes emerging within the sub-band. In this illustrative example, four frequencies are grouped into sub-band 1 (f_1, f_2) and 2 (f_3, f_4). Within each sub-band, the number of spikes in the two rows is summed up row-wisely. Thus the 4×5 dimension spike pattern is compressed into 2×5 . In this ideal case, the delays at all pure tones are all precisely detected as τ_2 . In a more realistic case, a spike pattern with local peaks and smooth slopes are more common.

C. Biological evidence of the MTPC

The aforementioned steps are pipelined to generate an integrated neural coding scheme for SSL, the MTPC. In this section, we aim to link the design of MTPC with biological evidence from neuroscience and anatomy.

Starting from the binaural case, two ears or microphones receive the acoustic signals x_1 and x_2 from two pathways, as demonstrated in Figure 1. After applying frequency analyzer in Eq. 1, each sensed sound wave is decomposed into pure

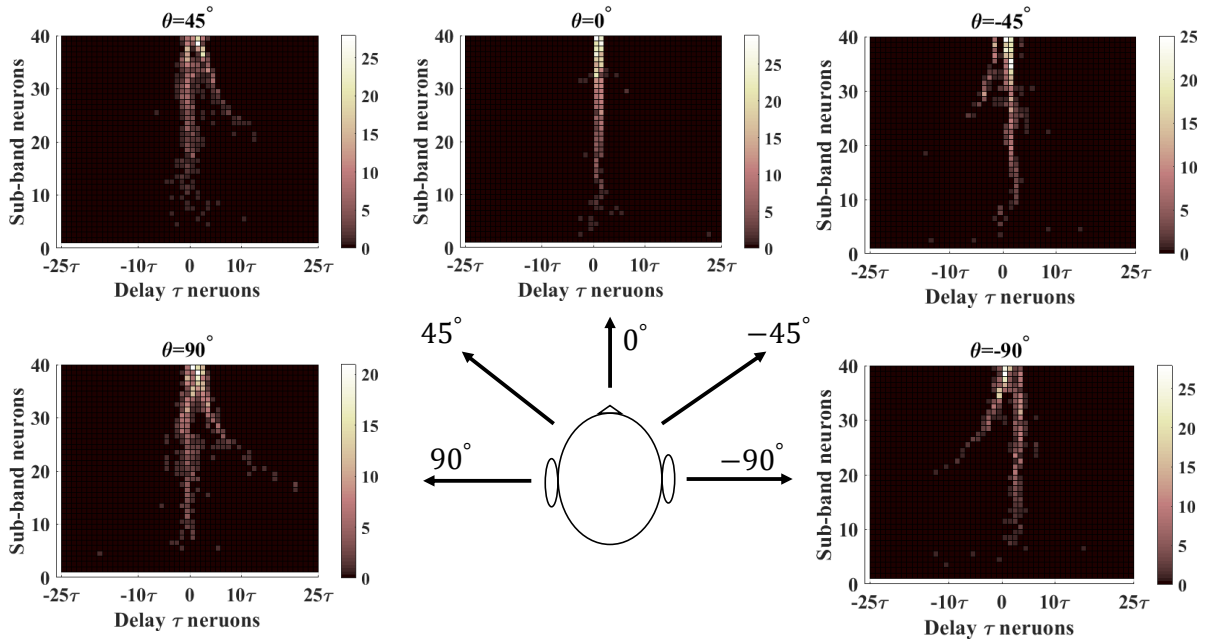


Figure 7. Real spike patterns that encode the location-dependent sounds from various azimuths

tones. Such a process imitates the tonotopic organization of the cochlea [28]. The basilar membrane, a stiff structural element within the cochlea [29], can respond to a certain frequency by some area along with it [30]. Such a distribution of single frequencies to various locations along the cochlea is called the tonotopic organization [31]. We note that the key to distinguishing the TDOA lies in the spatial variation of frequency responses in the tonotopic organization.

The next step is neural phase coding in Figure 4. The first peak of each tone is detected by the hair cells [32] in the cochlear and is encoded into a spatio-temporal pattern as in Figure 8, in which temporal axis represents the peaks' timings and the spatial axis represents the responding locations of the tonotopic organization, that is, the frequencies.

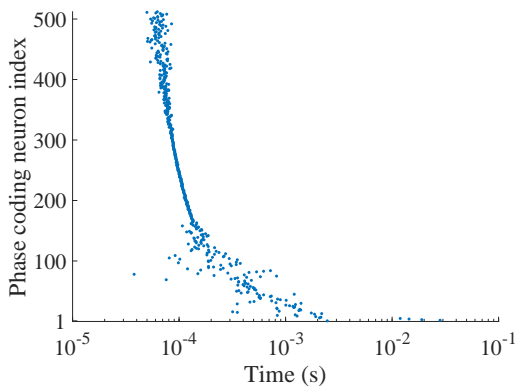


Figure 8. Output of neural phase coding. The input sound is decomposed into 512 pure tones, each tone is phase-coded by one neuron. The dots in this figure illustrate the firing timings of each encoding neuron.

After the neural phase coding, the couple of coded patterns from two ears are fed into the coincidence detection network (Figure 5). In this organization, pair-to-pair comparison of

each frequency is conducted, and the frequencies are still distinguished by the spatial variation. This organization is functionally inspired by the Jeffress's finding of delay lines [9], which anatomically locates at the medial superior olive (MSO) on the mammal's auditory pathway [5]. Finally the output layer of MTPC connects to the inferior colliculus (IC) [33] where the localization cues are decoded [34]. In this work, the function of IC is conducted by the spiking neural networks.

D. MTPC for a mixture of single tones: an instance for illustration

To better understand the mechanism of MTPC in both clean and noisy environments, we illustrate an instance in Figure 9, in which the stereo sounds are composed of four frequencies: 200Hz, 400Hz, 600Hz, and 800Hz. Each frequency tone shares the same energy level. In Figure 9(a) and (d), the binaural stereo sounds are received with a certain TDOA, in clean or noisy environments. Figure 9(b)(e) demonstrate the frequency analysis by the tonotopic organization of the cochlea, that is, the four frequency components are isolated in the time domain by stimulating the vibration of various areas in the basilar membrane. By observation, it is noted that for each frequency, the tones in (b) and (e) begin with different initial phases. It can be expected because the disturbance of white noise makes the phases shift on the sounds. However, what the MTPC scheme cares about is the phase difference between each binaural coupled tones with the same frequencies. Figure 9(c) and (f) shows the initial phases of (b) and (c) in a polar coordinate. Then we obtain the phase-difference for each couple of tones, shown in Figure 9(g), in which the green-colored circles and orange-colored triangles represent the clean and noisy cases. The noisy coupled tones have approximate phase-differences with the clean case, although their phases

are shifted by the disturbance of noise. The TDOA of each frequency f_{tone} will be simply derived by:

$$\delta t_{tone} = \frac{\delta \phi_{tone}}{2\pi f_{tone}} \quad (4)$$

where t_{tone} , ϕ_{tone} , and f_{tone} denote the TODA, phase difference, and frequency of the binaural coupled tones.

In conclusion, by analyzing the phase-differences in single-frequency tones, the TDOA is robust to the disturbance of noise. This point is crucial because for the conventional phase-locking coding strategy, the phase-differences of the original binaural sounds, or sub-band filtered outputs, are so vulnerable to the noise in the real environment that a robust TDOA can hardly be obtained. Such a problem makes the existing phase-lock coding based neural encoding front-ends for SSL only robust to a simple simulated scenario, rather in a real-world environment.

III. SPIKING NEURAL NETWORKS FOR AZIMUTH PREDICTION

The neural encoding MTPC scheme in Section II has successfully encoded the ITD cues into spatio-temporal spike patterns. The topology of the spike firings indicates the TDOA that is crucial for azimuth prediction. In this section, we aim to pipeline the encoded firing patterns with different architectures of SNNs, which serve as pattern classification models, to learn the ITD spiking representations and decode the sound source azimuths. To evaluate the universal applicability of the coding scheme, two diverse SNN strategies are exploited.

1) *Recurrent connections of LIF spiking neurons using back-propagation through time:* We first evaluate the encoded pattern in a recurrent connection of spiking neurons, the Recurrent Spiking Neural Network (RSNN). The recurrent connections of neurons are well approved to be prominent in dealing with temporal dynamic tasks. To optimize the Recurrent Neural Network (RNN), a commonly adopted synaptic updating approach is the back-propagation through time (BPTT).

The spiking neuron's internal dynamics of sub-threshold membrane potential $V(t)$ is modelled by the leaky integrate-and-fire (LIF) spiking neuron [35].

$$\tau_m \frac{dV(t)}{dt} = -V(t) + I(t) \quad (5)$$

where τ_m denotes the membrane constant. $I(t)$ represents the synaptic currents from both external input spikes and internal recurrent injection:

$$I(t) = \sum_i \omega_i^{\text{ext}} S^{\text{ext}}(t) + \omega^{\text{rec}} S^{\text{rec}}(t) \quad (6)$$

where ω and S represent the synaptic weights and input spike train, with superscript ext for external input and rec for internal recurrent injection. Once the membrane potential $V(t)$ exceeds the firing threshold θ , the spiking neuron will fire a spike. After that, the membrane potential is reset to 0, and the neuron enters a refractory period during which it cannot spike.

When we organize the aforementioned spiking neurons in a recurrent connection, the Recurrent Spiking Neural Network

(RSNN) is defined [36]. The synaptic updating rule, which is the backpropagation in recurrent LIF neurons through time, is slightly different from conventional BPTT because the output spike train $z(t)$ of LIF neurons are non-differential. Therefore, researchers propose [37] the pseudo-derivative as a solution and it is proved effective [36], [38].

$$\frac{dz(t)}{dV(t)} = \max \left\{ 0, 1 - \left| \frac{V(t) - \theta}{\theta} \right| \right\} \quad (7)$$

where $z(t)$ and $V(t)$ denote the output spike train and membrane potential of an LIF spiking neuron.

2) *Convolutional spiking neural network (CSNN) using spatio-temporal backpropagation:* We also utilize the convolutional connections of LIF spiking neurons (Eq.5-6), the CSNN, to evaluate our MTPC scheme. The synaptic updating rule of SCNN follows [39], in which the pseudo-derivative Eq.7 is also used in the propagation of gradients.

IV. EXPERIMENT

One of the main superiority of MTPC over the conventional neuromorphic models [16], [17], [19]–[22], [26], [27], is that the MTPC is designed with robustness to noise, as illustrated in Figure 9. For evaluating the effectiveness in a noisy real-world environment, we have collected our localization dataset using a microphone array; The experiment results evaluate the MTPC scheme in a challenging real-world environment.

A. Real-world collected dataset for precise SSL

The data collection equipment's set-up is illustrated in Figure 11. A microphone array, which locates on top of a robotic platform, records the sounds from a loudspeaker. The loudspeaker moves along the circle to emit stereo sounds from different azimuths.

The ReSpeaker microphone array is applied in the SSL data collection and its settings are illustrated in Figure 10. Four microphones, automatically synchronized, record the sounds at 16kHz sampling rate from the loudspeaker and save the waveforms into .wav format files. The 0° is defined at the center of Mic 3 and Mic 4, and it increases in counterclockwise to 355° . The contents of sounds are speech voice from RSR2015 corpus [40], by which we aim to imitate the oral orders to the robot.

In the data collection phase, the multi-functional robot platform serves as a power supplier and support to the ReSpeaker, which stands on the center of the robot. The azimuths are marked on the ground with two distances: 1.0m and 1.5m, as the two circles shown in Figure 11. It is also noted that the center of the microphone array overlaps at the center of the marked circles.

For a constant SNR, the volume of the loudspeaker at 1.5m is set to the maximal value, while it is $\frac{1^2}{1.5^2} \approx 44\%$ of the maximum at 1.0m, according to the inverse square law of wave propagation.

The numerical details of the collected data are shown in Table I. Approximately a total of 15 hours of recordings are collected, and they are clipped into 170ms per sample, with a stride size of 85ms. For each azimuth, the average

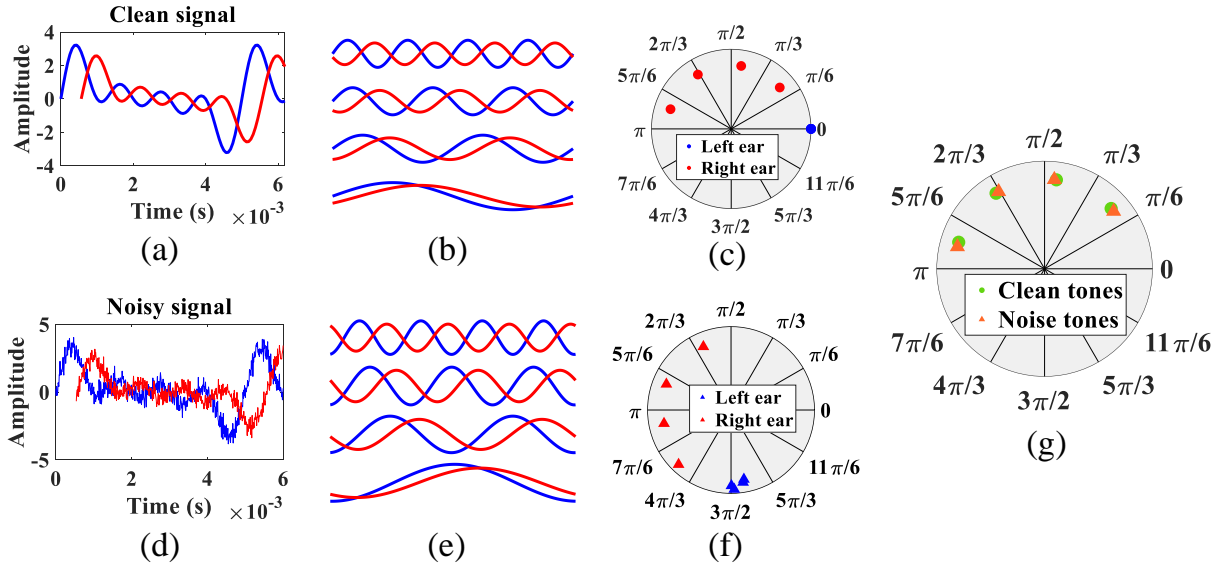


Figure 9. The illustration of the phase differences of pure-tone signals. A sound source generates a composed sound with four frequency components of 200Hz, 400Hz, 600Hz, 800Hz. The ideal clean case and real-world noisy case are (a) and (d). By the MTPC scheme, the noisy case can still maintain the phase-differences, from which the TDOA will be directly obtained.

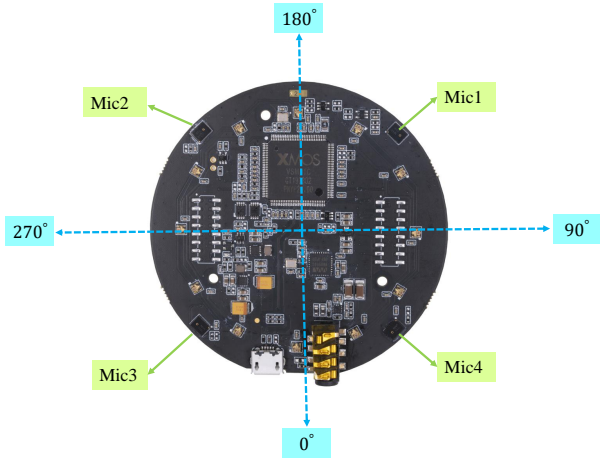


Figure 10. The ReSpeaker Microphone array and its settings for the data collection experiment.

Parameters	Values
Sampling frequency	16kHz
Num of mic channels	4
Distance	1.0m, 1.5m
Speech corpus	RSR2015 [40]
Azimuth range	[0°, 355°]
Azimuth resolution	5°
Total recording time	15h
Sample duration	170ms
Ave training samples/degree°	1848
Ave testing samples/degree°	344

Table I THE NUMERICAL DETAILS OF THE COLLECTED SSL DATASET.

numbers of training and testing samples are 1848 and 344. The azimuth resolution is 5°, which is smaller than any known neuromorphic SSL system [16], [17], [19]–[22], [26], [27], which also challenges our proposed model.

B. Integrated spiking-based SSL system for real-world applications

1) *Extend from two ears to a microphone array:* The MTPC is inspired by the mammal’s binaural auditory pathway for SSL, and explained in the binaural case, though, its mathematical principle makes it easily extended to a microphone array case, in which topological multiple microphones (> 2) receive stereo sounds synchronously.

In the experimental microphone array case, we can regard each pair of mics as one binaural case, and combine them as one individual spike pattern. The reasons are that different mic pairs provide various TDOA features, due to various locations relative to the sound source; and the combination of these features will contribute to estimate the sound source in 360° azimuth.

2) *Apply MTPC to various SNN back-ends:* In this 4-mic case in Figure 10, a total of $C_4^2 = 6$ pairs of binaural spike patterns will be achieved. How to combine them into one

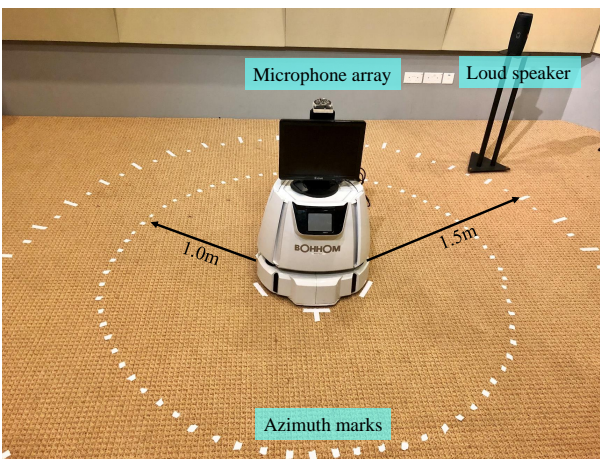


Figure 11. The equipment’s set-up for the SSL data collection.

Parameters	Values
Number of FFT points	1024
Number of analytical pure tones	512
Cochlear filter channels	20, 40
TDOA resolution	0.0625ms

Table II
THE PARAMETERS OF MTPC IN THE SSL EXPERIMENT.

pattern depends on the architectures of SNN back-ends. Let's take the CSNN and RSNN as an instance.

Figure 12 illustrates the approach to pipeline the MTPC with different SNN architectures. The 4-channel acoustic sample in Figure 12(a) is encoded by MTPC into six spike patterns. The six patterns are combined by two approaches:

For the convolutional SNN, the six 2-D spike patterns are stacked into a 3-D spike pattern, shown in Figure 12(c), in which the third dimension is along with the index (1 to 6) of the 2-D patterns. In this case, the encoded neurons are organized in 3 dimensions: the time delay dimension, the frequency channel dimension, and the index of the 2-D patterns dimension.

For the recurrent SNN, the six patterns are tandemed along the time delay dimension, as in Figure 12(d). In this case, the number of RSNN input neurons are the same as the number of frequency channels. Therefore, each row of the newly combined spike pattern is fed into each input neuron, and the values (the spike counts) are converted into the input current intensities at each time step of the recurrent network.

The network architectures of CSNN and RSNN are summarized in Table III. The input layers are corresponding to the dimensions of the MTPC encoded spike patterns; the output layers are both 1×360 output neurons. The firing rates of the neurons in the output layer indicate the estimated possibilities of sound source's azimuth in each angle around 360° . The Mean Square Error (MSE) loss function is defined as:

$$L_{MSE} = \frac{1}{360} \sum_{i=1}^{360} (\mathcal{L}_i - \mathcal{O}_i)^2 \quad (8)$$

where \mathcal{L} and \mathcal{O} denote the 1×360 dimensional SNN output and the Gaussian azimuth label curve, respectively. The Gaussian label curve is defined as a 360° cyclic normalized Gaussian-shaped curve centered at the azimuth label. At the end, a peak detection block (Figure 12(e)) detects the peak of the possibility curve and decides the estimated azimuth in degree.

C. Localization Accuracy in Different Detection Environments and set-up

To thoroughly investigate the effectiveness of MTPC, we evaluate the scheme in various experimental environments and compare it with other state-of-the-art SSL algorithms or network models for benchmarking, in terms of Mean Absolute Error (MAE):

$$MAE = \frac{1}{N_{sa}} \sum_{i=1}^{N_{sa}} |a_{Estimate} - a_{Label}| \quad (9)$$

where $a_{Estimate}$, a_{Label} , and N_{sa} denote the estimated angle and the label angle in degree, and the number of testing samples, respectively.

1) *Distribution of MAE on different number of coincidence detectors*: In the design of MTPC, we introduce the coincidence detection network (Figure 5) for projecting the ITD of each pure tones onto the delay lines. Given the number of pure tones and frequency channels, the encoded pattern's scale is decided by the number of coincidence detectors, or delay lines. Assuming the number of coincidence detectors is $2d + 1$ and sampling rate of f_s , the ITD detection ranges in $[-d\frac{1}{f_s}, -(d-1)\frac{1}{f_s}, \dots, -\frac{1}{f_s}, 0, \frac{1}{f_s}, \dots, d\frac{1}{f_s}]$. Therefore, it is predictable that a wider scale of coincidence detectors will offer a wider range of ITD detection. On the other hand, a larger scale of patterns will bring more computational cost to the SNN and might degrade the performance of it.

We aim to investigate the proper scale of the coincidence detection network, by evaluating the localization accuracy under different numbers of coincidence detectors. Figure 13 demonstrates the MAE as a function of coincidence detector numbers. We test from 11 to 61 coincidence detectors, which means a detection range from $-0.3125 \sim 0.3125$ ms to -1.8750 ms ~ 1.8750 ms.

We note that the optimal scale of the coincidence detection network is at 51 delay lines, which effectively and efficiently detects the ITD of -1.5625 ms ~ 1.5625 ms.

2) *MAE on different frequency channels*: In Figure 6, the coincidence-detected pure tones are grouped into frequency channels. We evaluate two cases: 20 channels and 40 channels, for finding the optimal scale of the encoded pattern. Table IV shows the SSL accuracy of both cases, by different SNN back-ends. The 40-channel MTPC offers a lower MAE than the 20-channel case.

3) *Distribution of MAE on 360° of all azimuths*: A satisfying SSL system is supposed to perform stably on any direction, rather than on some particular ones or ranges. Figure 14 illustrates the MAE distribution on 360° . At the experimental distance of 1.5m, the results show the MAEs of MTPC with CSNN and RSNN. The MAEs of both models keep lower than 2° and, more importantly, the MAE performances show no significant difference across all directions. It indicates that: firstly the MTPC scheme achieves stable performance on any direction; and it is extended successfully from binaural to microphone array case.

4) *Compare the MTPC-SNN models with other state-of-the-art SSL algorithms*: We have already investigated the characteristics of the MTPC itself. Now let's move to compare its performance with the other state-of-the-art SSL systems. We make two comparisons:

Firstly, evaluated by the same location-dependent dataset in Section IV-A, the proposed MTPC with various SNN back-ends are compared with two most commonly used non-neuromorphic SSL approaches: the general cross-correlation phase transform (GCC-Phat) [41] and the multiple signal classification (MUSIC) [42] for benchmarking. Experiment results are summarized in Table V.

Compared with the other non-neuromorphic algorithms, our MTPC-SNN models outperform them in both 1.5m and 1.0m

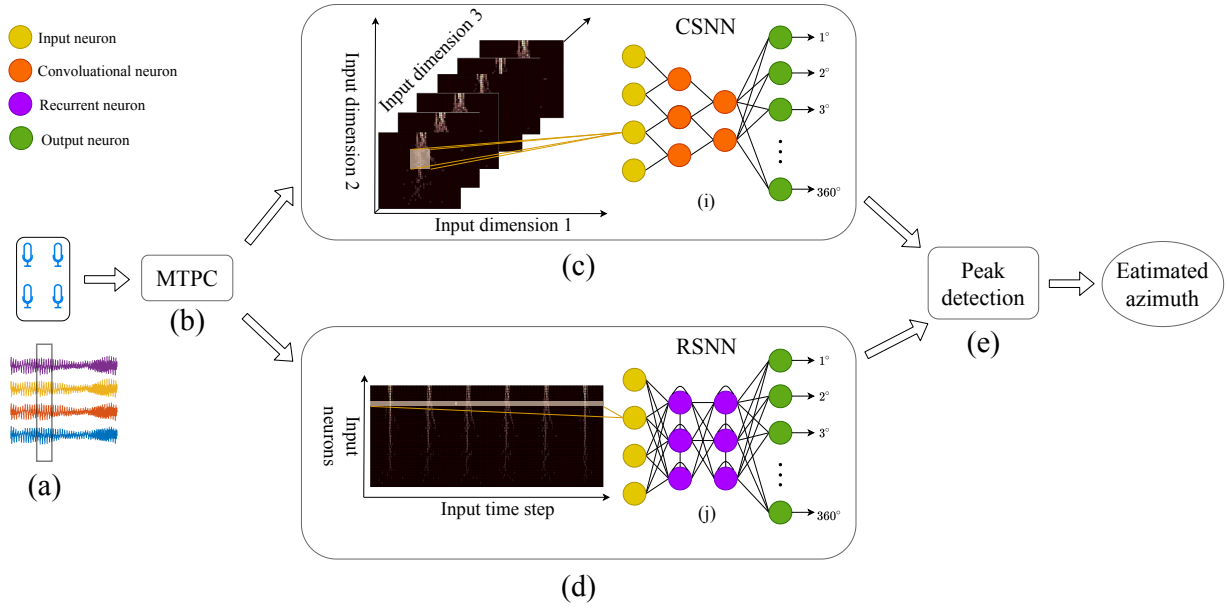


Figure 12. Apply MTPC with different SNN structures:the recurrent SNN (RSNN) and convolutional SNN (CSNN)

Spiking neuron connection	Input layer	Hidden layer	Output layer
CSNN	$51 \times 6 \times 40$	12c3s2p1 24c3s2p1 - 48c3s2p1 96c3s2p1 - fc512	1×360
RSNN	1×40	r1024	1×360

Table III
THE ARCHITECTURE OF SNN BACK-ENDS.

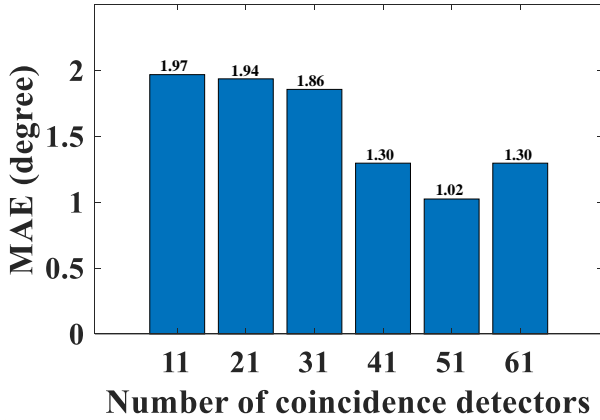


Figure 13. The MAE as a function of different numbers of coincidence detection neurons.

SNN models	MAE° for 20-channel MTPC	MAE° for 40-channel MTPC
CSNN	1.95	1.61
RSNN	1.60	1.02

Table IV

THE MAES RESULTS ON 20 AND 40 COCHLEAR FREQUENCY CHANNELS.

distances. Our 40-channel MTPC-RSNN models achieve the minimal MAE of 1.02°. Besides, the MTPC is also pipelined with the conventional ANN back-ends, the convolutional neural network [43] and long short term memory (LSTM) network [44], making some semi-neuromorphic approaches. It is noted that the MTPC-LSTM performs the best because conventional

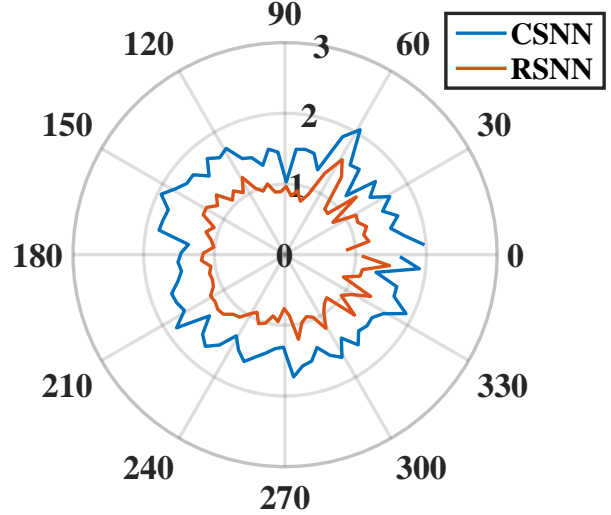


Figure 14. The distribution of MAE on 360° all directions, at distance of 1.5m.

Neural Encoding	Network back-ends	MAE° for 1.5m	MAE° for 1.0m
MTPC	CSNN [39]	1.61	4.84
	RSNN [36]	1.02	4.09
	CNN [43]	1.20	4.06
	LSTM [44]	0.41	3.89
Other SSL Algorithms			
	GCC-Phat + CNN [41]	1.57	4.38
	MUSIC [42]	2.35	3.79

Table V

MAES RESULTS ON VARIOUS SNN BACK-ENDS, AND COMPARING WITH OTHER BENCHMARKING SSL APPROACHES.

ANN's ability as classification back-ends is better than that of the SNN, which means proposing more effective learning algorithms for SNN still leaves as an open question.

Secondly, we make a parallel comparison with the other state-of-the-art neuromorphic approaches for SSL. The experimental datasets are simulated or collected by the authors themselves, though, we can compare the complexity and achievements of these works to draw some conclusions. They are summarized in Table VI.

We first pay attention to whether their proposed models are purely neuromorphic from spike encoding front-end to SNN back-ends, or semi-neuromorphic with half spiking approaches. It has been mentioned that a purely spike-involved system can fully show all the advantages of neuromorphic computing, such as low power consumption, processing of temporal information, etc. Only

The complexity of the dataset is evaluated in terms of a larger detection range of azimuth, higher resolution (the minimal distinguished angle), real-world data source other than artificially simulated, and sound types with more frequency components.

The results are reported in two forms: the correct percentage in some resolution, or MAE. Our 40-channel MTPC-RSNN model outperforms the others and achieves both the highest resolution accuracy and lowest MAE.

5) *MAE in noisy environments*: Finally, the robustness of the proposed model is examined under various conditions of noisy conditions.

Figure 15 shows the MAEs as a function of the Signal-to-Noise Ratio (SNR). Three types of background noise: the indoor crowd noise, factory machine noise, and outdoor traffic noise are used to evaluate the performances in near-field indoor, far-field indoor, and far-field outdoor application scenarios.

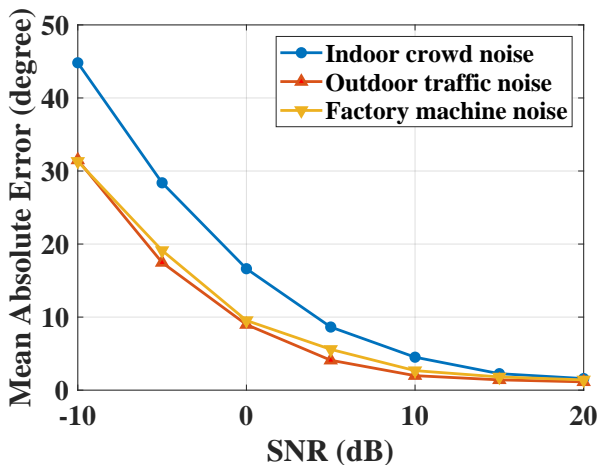


Figure 15. The MAE as a function of background noise SNR. The experimental SSL model is 40-channel MTPC-RSNN. The noise robustness is examined under three different types of noise, corresponding to three application scenes in which the SSL systems are usually working.

Our SSL system performs well ($MAE \leq 10^\circ$) at $SNR \geq 0dB$. But its accuracy slightly degrades under the indoor crowd noisy environment. This might be because the system

is trained with speech-based stereo dataset, thus the system is sensitive to human voices. Furthermore, speech voices have richer and more dynamic frequency components, compared with the traffic or machine noise.

The next experimental scenario is the directional noise of human speech. The sound from the detected source is disturbed by the sounds from other directions. In this experiment, we arrange the disturbance source of speech voice at 1.5m distance, randomly from one of the four directions: 0° , 90° , 180° , 270° .

The experiment is conducted by conditional training. According to the SNR, the directional noise are grouped into two levels: high-noise (0-5dB) and low-noise (15-20dB). The conditional training means that the SSL model is trained and tested with noisy data from the same noise condition level. And the clean training means that the model is trained with noiseless data and tested with noisy data.

This SSL system is also designed to be applied in the robotic platform, that receives the oral orders of human speech. As such, the robustness to the directional human voice noise is significant. The results in Table VII indicate the effectiveness of conditional training, in which MAE drops a lot at a high-noise level. Conditional training of the SSL system offers us an effective solution to directional noise.

V. DISCUSSION

The MTPC scheme is independent of the types of synaptic learning rules, no matter they are rate-based or temporal-based; and also independent of the architectures of SNN, no matter recurrent or convolutional connections. The principle of MTPC is, by following the auditory pathway of mammals, to project the implicit ITD cues onto the time-delay dimension and frequency-channel dimension (Figure 7), which explicitly demonstrates the distribution of TDOA across various frequency sub-bands. The values of the pattern, interpreted in mathematics, represent the confidence of the particular TDOA. If they are interpreted in a neuronal system, the values could be either spike rates (for rate-based SNN) or synaptic currents (for temporal-based SNN), by which the higher values means the more intensive inputs. Furthermore, as long as the time-delay dimension is preserved, the spiking pattern is compatible with most sorts of SNN architectures, which is proved by CSNN and RSNN in the experiments.

We note that the MAEs for 1.0m are always higher than those for 1.5m (Table IV, V), which might be counter-intuitive. This is because the loudspeaker occupies some space (Figure 11), which covers a range of azimuth when the distance is nearer. Therefore, the data labeling is not accurate, since it is not distinguishable at such a fuzzy range. Nevertheless, considering the detection distance, the MAE of $\sim 5^\circ$ is sufficiently accurate.

VI. CONCLUSION

In this paper, we propose a novel neural encoding scheme: the Multi-Tones' Phase Coding for the SNN-based SSL task. This MTPC is able to encode the input raw waveforms, either from ears or microphone array, into spike patterns that are

Proposed by	Spike front-end	SNN back-end	Azimuth range	Resolution	Date source	Sound type	Results
Xiao, Feng, et al. [20]	yes	no	-90° ~ 90°	10°	HRTF	Pure tones	74.56%(±10°)
Wall, Julie A., et al. [7]	yes	yes	-60° ~ 60°	10°	HRTF	Pure tones	95.38%(±10°)
Voutsas, Kyriakos, et al. [22]	yes	no	-45° ~ 45°	15°	Microphone data	pure tones	72.50%(±15°)
Liu, Jindong, et al. [23]	yes	no	-45° ~ 45°	10°	HRTF	Speech	90.00%(±10°)
Goodman, Dan, et al. [25]	yes	no	-180° ~ 180°	15°	HRTF	Speech, sounds	4° ~ 8° MAE
Dvila-Chacn, Jorge, et al. [45]	yes	no	-90° ~ 90°	15°	Microphone data	Speech	91.00%(±15°)
Anumula, Jithendar, et al. [46]	yes	no	-180° ~ 180°	30°	Microphone data	Speech	80.00%(±30°)
40-channel MTPC-RSNN (this work)	yes	yes	-180° ~ 180°	5°	Microphone data	Speech	~ 100%(±5°) or 1.02° MAE

Table VI

SUMMARY OF THE STATE-OF-THE-ART NEUROMORPHIC APPROACHES FOR SSL. THE COMPARISON IS BASED ON THE COMPLEXITIES OF THE DATASETS AND THE ACHIEVEMENTS OF THE SSL TASKS.

Testing SNR (dB)	0	5	10	15	20
Clean training	54.84	33.93	12.64	8.75	3.88
Conditional training	10.75	6.83	—	1.76	1.07

Table VII

THE MAE OF CONDITIONAL TRAINING IN DIFFERENT DIRECTIONAL NOISE SNR. THE ACOUSTIC DISTURBANCE OF HUMAN SPEECH RANDOMLY COMES FROM ONE OF THE FOUR DIRECTIONS: 0°, 90°, 180°, 270°.

compatible with most of the existing SNN architectures and synaptic learning methods. The significance of this work is achieving a purely neuromorphic computational model that fully owns the advantages over the ANN models, superior to the other semi-neuromorphic approaches. Moreover, our model outperforms the other SNN-based models, in terms of the dataset complexity, detection range, localization accuracy, etc.

ACKNOWLEDGMENT

This research is supported by Programmatic grant no. A1687b0033 from the Singapore Governments Research, Innovation and Enterprise 2020 plan (Advanced Manufacturing and Engineering domain)

REFERENCES

- [1] C. H. Brown and B. J. May, "Comparative mammalian sound localization," in *Sound source localization*. Springer, 2005, pp. 124–178.
- [2] B. Grothe, M. Pecka, and D. McAlpine, "Mechanisms of sound localization in mammals," *Physiological reviews*, vol. 90, no. 3, pp. 983–1012, 2010.
- [3] S. P. Thompson, "Li. on the function of the two ears in the perception of space," *The London, Edinburgh, and Dublin Philosophical Magazine and Journal of Science*, vol. 13, no. 83, pp. 406–416, 1882.
- [4] J. W. Strutt, "On our perception of sound direction," *Philosophical Magazine*, vol. 13, no. 74, pp. 214–32, 1907.
- [5] T. Yin and J. Chan, "Interaural time sensitivity in medial superior olive of cat," *Journal of neurophysiology*, vol. 64, no. 2, pp. 465–488, 1990.
- [6] D. J. Tollin, "The lateral superior olive: a functional role in sound source localization," *The neuroscientist*, vol. 9, no. 2, pp. 127–143, 2003.
- [7] J. A. Wall, L. J. McDaid, L. P. Maguire, and T. M. McGinnity, "Spiking neural network model of sound localization using the interaural intensity difference," *IEEE transactions on neural networks and learning systems*, vol. 23, no. 4, pp. 574–586, 2012.
- [8] T. C. Yin, "Neural mechanisms of encoding binaural localization cues in the auditory brainstem," in *Integrative functions in the mammalian auditory pathway*. Springer, 2002, pp. 99–159.
- [9] L. A. Jeffress, "A place theory of sound localization," *Journal of comparative and physiological psychology*, vol. 41, no. 1, p. 35, 1948.
- [10] C. E. Carr and M. Konishi, "Axonal delay lines for time measurement in the owl's brainstem," *Proceedings of the National Academy of Sciences*, vol. 85, no. 21, pp. 8311–8315, 1988.
- [11] C. Carr and M. Konishi, "A circuit for detection of interaural time differences in the brain stem of the barn owl," *Journal of Neuroscience*, vol. 10, no. 10, pp. 3227–3246, 1990.
- [12] J. K. Moore, "Organization of the human superior olivary complex," *Microscopy research and technique*, vol. 51, no. 4, pp. 403–412, 2000.
- [13] M. Lewicki, "Sound localization 1," *Computational Perception and Scene Analysis Module, Carnegie Mellon University*, <http://www.cs.cmu.edu/~lewicki/epsa/soundlocalization1.pdf>, 2006.
- [14] R. Levine, J. Gardner, S. Stufflebeam, B. Fullerton, E. Carlisle, M. Furst, B. Rosen, and N. Kiang, "Binaural auditory processing in multiple sclerosis subjects," *Hearing research*, vol. 68, no. 1, pp. 59–72, 1993.
- [15] M. Furst, V. Aharonson, R. A. Levine, B. C. Fullerton, R. Tadmor, H. Pratt, A. Polyakov, and A. D. Korczyn, "Sound lateralization and interaural discrimination: Effects of brainstem infarcts and multiple sclerosis lesions," *Hearing research*, vol. 143, no. 1-2, pp. 29–42, 2000.
- [16] J. A. Wall, L. J. McDaid, L. P. Maguire, and T. M. McGinnity, "Spiking neuron models of the medial and lateral superior olive for sound localisation," in *2008 IEEE International Joint Conference on Neural Networks (IEEE World Congress on Computational Intelligence)*. IEEE, 2008, pp. 2641–2647.
- [17] B. Glackin, J. A. Wall, T. M. McGinnity, L. P. Maguire, and L. J. McDaid, "A spiking neural network model of the medial superior olive using spike timing dependent plasticity for sound localization," *Frontiers in computational neuroscience*, vol. 4, p. 18, 2010.
- [18] F. Ponulak, "Resume-new supervised learning method for spiking neural networks. institute of control and information engineering, poznań university of technology," Tech. rep, Tech. Rep., 2005.
- [19] E. C. Escudero, F. P. Peña, R. P. Vicente, A. Jimenez-Fernandez, G. J. Moreno, and A. Morgado-Estevez, "Real-time neuro-inspired sound source localization and tracking architecture applied to a robotic platform," *Neurocomputing*, vol. 283, pp. 129–139, 2018.
- [20] F. Xiao and D. Weibei, "A biologically plausible spiking model for interaural level difference processing auditory pathway in human brain," in *2016 International Joint Conference on Neural Networks (IJCNN)*. IEEE, 2016, pp. 5029–5036.
- [21] R. Luke and D. McAlpine, "A spiking neural network approach to auditory source lateralisation," in *ICASSP 2019-2019 IEEE International Conference on Acoustics, Speech and Signal Processing (ICASSP)*. IEEE, 2019, pp. 1488–1492.
- [22] K. Voutsas and J. Adamy, "A biologically inspired spiking neural network for sound source lateralization," *IEEE transactions on Neural Networks*, vol. 18, no. 6, pp. 1785–1799, 2007.
- [23] J. Liu, D. Perez-Gonzalez, A. Rees, H. Erwin, and S. Wermter, "A biologically inspired spiking neural network model of the auditory midbrain for sound source localisation," *Neurocomputing*, vol. 74, no. 1-3, pp. 129–139, 2010.
- [24] J. Dávila-Chacón, J. Liu, and S. Wermter, "Enhanced robot speech recognition using biomimetic binaural sound source localization," *IEEE transactions on neural networks and learning systems*, vol. 30, no. 1, pp. 138–150, 2018.
- [25] D. F. Goodman and R. Brette, "Spike-timing-based computation in sound localization," *PLoS computational biology*, vol. 6, no. 11, p. e1000993, 2010.
- [26] D. Goodman and R. Brette, "Learning to localise sounds with spiking neural networks," in *Advances in Neural Information Processing Systems*, 2010, pp. 784–792.
- [27] D. F. Goodman, V. Benichoux, and R. Brette, "Decoding neural responses to temporal cues for sound localization," *Elife*, vol. 2, p. e01312, 2013.

- [28] T. R. Bourk, J. P. Mielcarz, and B. E. Norris, "Tonotopic organization of the anteroventral cochlear nucleus of the cat," *Hearing research*, vol. 4, no. 3-4, pp. 215–241, 1981.
- [29] M. A. Ruggero, "Responses to sound of the basilar membrane of the mammalian cochlea," *Current opinion in neurobiology*, vol. 2, no. 4, pp. 449–456, 1992.
- [30] M. A. Ruggero, N. C. Rich, A. Recio, S. S. Narayan, and L. Robles, "Basilar-membrane responses to tones at the base of the chinchilla cochlea," *The Journal of the Acoustical Society of America*, vol. 101, no. 4, pp. 2151–2163, 1997.
- [31] T. Holton and A. Hudspeth, "A micromechanical contribution to cochlear tuning and tonotopic organization," *Science*, vol. 222, no. 4623, pp. 508–510, 1983.
- [32] W. E. Brownell, C. R. Bader, D. Bertrand, and Y. De Ribaupierre, "Evoked mechanical responses of isolated cochlear outer hair cells," *Science*, vol. 227, no. 4683, pp. 194–196, 1985.
- [33] H. Faye-Lund and K. K. Osen, "Anatomy of the inferior colliculus in rat," *Anatomy and embryology*, vol. 171, no. 1, pp. 1–20, 1985.
- [34] J. A. Winer, D. T. Larue, J. J. Diehl, and B. J. Hefti, "Auditory cortical projections to the cat inferior colliculus," *Journal of Comparative Neurology*, vol. 400, no. 2, pp. 147–174, 1998.
- [35] R. Brette and W. Gerstner, "Adaptive exponential integrate-and-fire model as an effective description of neuronal activity," *Journal of neurophysiology*, vol. 94, no. 5, pp. 3637–3642, 2005.
- [36] G. Bellec, D. Salaj, A. Subramoney, R. Legenstein, and W. Maass, "Long short-term memory and learning-to-learn in networks of spiking neurons," in *Advances in Neural Information Processing Systems*, 2018, pp. 787–797.
- [37] M. Courbariaux, I. Hubara, D. Soudry, R. El-Yaniv, and Y. Bengio, "Binarized neural networks: Training deep neural networks with weights and activations constrained to+ 1 or-1," *arXiv preprint arXiv:1602.02830*, 2016.
- [38] S. K. Esser, P. A. Merolla, J. V. Arthur, A. S. Cassidy, R. Appuswamy, A. Andreopoulos, D. J. Berg, J. L. McKinstry, T. Melano, D. R. Barch *et al.*, "From the cover: convolutional networks for fast, energy-efficient neuromorphic computing," *Proceedings of the National Academy of Sciences of the United States of America*, vol. 113, no. 41, p. 11441, 2016.
- [39] Y. Wu, L. Deng, G. Li, J. Zhu, Y. Xie, and L. Shi, "Direct training for spiking neural networks: Faster, larger, better," in *Proceedings of the AAAI Conference on Artificial Intelligence*, vol. 33, 2019, pp. 1311–1318.
- [40] A. Larcher, K. A. Lee, B. Ma, and H. Li, "Text-dependent speaker verification: Classifiers, databases and rsr2015," *Speech Communication*, vol. 60, pp. 56–77, 2014.
- [41] W. He, P. Motlicek, and J.-M. Odobez, "Deep neural networks for multiple speaker detection and localization," in *2018 IEEE International Conference on Robotics and Automation (ICRA)*. IEEE, 2018, pp. 74–79.
- [42] R. Schmidt, "Multiple emitter location and signal parameter estimation," *IEEE transactions on antennas and propagation*, vol. 34, no. 3, pp. 276–280, 1986.
- [43] Y. LeCun, Y. Bengio *et al.*, "Convolutional networks for images, speech, and time series," *The handbook of brain theory and neural networks*, vol. 3361, no. 10, p. 1995, 1995.
- [44] S. Hochreiter and J. Schmidhuber, "Long short-term memory," *Neural computation*, vol. 9, no. 8, pp. 1735–1780, 1997.
- [45] J. Dávila-Chacón, S. Heinrich, J. Liu, and S. Wermter, "Biomimetic binaural sound source localisation with ego-noise cancellation," in *International Conference on Artificial Neural Networks*. Springer, 2012, pp. 239–246.
- [46] J. Anumula, E. Ceolini, Z. He, A. Huber, and S.-C. Liu, "An event-driven probabilistic model of sound source localization using cochlea spikes," in *2018 IEEE International Symposium on Circuits and Systems (ISCAS)*. IEEE, 2018, pp. 1–5.